PERINATAL CHANGES IN FETAL VENTRICULAR GEOMETRY, MYOCARDIAL PERFORMANCE AND CARDIAC FUNCTION IN NORMAL TERM PREGNANCIES

Olga Patey MD*†‡, Michael A. Gatzoulis MD PhD FACC FESC §||,

Basky Thilaganathan MD PhD FRCOG*† and Julene S. Carvalho MD PhD FRCPCH*†‡#

Molecular & Clinical Sciences Research Institute, St George's University of London, UK*;

Fetal Medicine Unit, St. George's Hospital, London, UK†;

Brompton Centre for Fetal Cardiology, Royal Brompton Hospital, London, UK‡;

National Institute for Health Research Cardiovascular Biomedical Research Unit, Royal Brompton Hospital, London, UK§;

National Heart and Lung Institute, Imperial College London, London, UK ||;

Joint last authors#

Author for correspondence

Dr. Olga Patey

Fetal Medicine Unit, Lanesborough Wing

St. Georges Hospital NHS Foundation Trust

London SW17 0QT

Telephone: +44 20 8725 0071

Fax: +44 20 8725 0079

Email: pateyolga@gmail.com

Abbreviations: AVV=atrio-ventricular valve; CO=cardiac output; EDD=end-diastolic dimension; ESD=end-systolic dimension; IVS=inter-ventricular septal; LV=left ventricular; MPI=myocardial performance index; RV=right ventricular; STI=speckle tracking imaging; SV=stroke volume; TDI=tissue Doppler imaging.

ABSTRACT

Background: The fetal heart at term is exposed to an increase in hemodynamic work as a consequence of fetal growth, increased circulating volume and alteration in loading patterns due to maturational changes in fetoplacental circulation. The extent to which these cardiovascular changes influence the human fetal and neonatal cardiac adaptation has not been fully elucidated. The aim of this study was to evaluate perinatal cardiovascular changes in ventricular geometry and myocardial performance in normal term fetuses.

Methods: Prospective study of 108 uncomplicated pregnancies delivering at term. M-mode, two-dimensional (2D) or B-mode, pulsed wave (PW) Doppler, PW tissue Doppler and 2D speckle tracking imaging were performed a few days before, and within 24 hours of birth.

Results: Analysis of paired fetal and neonatal echoes demonstrated significant perinatal changes ($p<0.0001$ for all) in right ventricular (RV) and left ventricular (LV) geometry (RV/LV end-diastolic dimension ratio: 1.2 vs. 0.8, RV sphericity index: 0.53 vs. 0.40, LV sphericity index: 0.46 vs. 0.49). There were corresponding significant ($p<0.001$ for all) perinatal changes in global myocardial performance: LV myocardial performance index (MPI'): 0.60 vs. 0.47, RV MPI': 0.61 vs. 0.42; systolic function: LV longitudinal systolic strain rate: -1.4 /s vs. -1.0 /s, RV longitudinal systolic strain rate: -1.5 /s vs. -1.0 /s; RV systolic annular peak velocity (S'): 5.3 cm/s vs. 6.5 cm/s; and diastolic function: LV diastolic annular peak velocity ratio (E'/A'): 0.8 vs.1.1.

Conclusion: The findings support the concept that the perinatal period is associated with major changes in fetal ventricular geometry and cardiac function in response to significant alterations in loading conditions. Improved knowledge of perinatal cardiac changes in normal fetuses could facilitate better understanding of cardiac adaptation in normal and pathological pregnancies.

Key Words: fetal echocardiography; fetal heart; myocardial performance index; perinatal loading conditions; speckle tracking; tissue Doppler imaging.

INTRODUCTION

As the heart grows and develops *in utero*, it is exposed to an increase in hemodynamic work as a consequence of fetal growth, increased circulating volume, and alteration in loading patterns due to maturational changes in fetal and placental circulation. The developing heart may therefore be subject to considerable changes in ventricular geometry, myocardial performance and cardiac function, especially at near term. The right ventricle is a dominant chamber in fetal life supplying the lower body organs with less oxygenated blood through the ductus arteriosus (1). The left ventricular output directs more oxygenated through the ascending aorta to the upper body feeding the coronary and cerebral circulation. In this parallel fetal circulation, both ventricles are in communication with the descending aorta (1), have similar systolic pressures but are still subject to different afterloads. Dramatic changes occur at birth with closure of the prenatal shunts, lowering of the pulmonary vascular resistance, increase in systemic vascular resistance and with the two ventricles now functioning in series. Although previous workers have explored this phenomenon in animal models (2), only few early (3-6) and recent (7-10) human studies have investigated the extent to which these cardiovascular changes influence the human perinatal cardiac adaptation and produced conflicting results.

A comprehensive assessment of the fetal heart at term may help to improve the understanding of perinatal fetal cardiac adaptation in normal and pathological pregnancies. Strain and strain rate analysis by tissue Doppler (TDI) and speckle tracking (STI) imaging has been found to have a stronger correlation to invasive indices of myocardial performance, a higher sensitivity for detecting even mild myocardial damage and a stronger predictive value for cardiovascular complications than conventional echo indices (11, 12). In spite of these newer techniques for cardiac imaging, there are few studies using these methods to assess perinatal fetal heart function in normal term pregnancies (8-10). The aim of this study was to characterise cardiac geometry and function in normal term fetuses and neonates, and how perinatal changes in loading conditions may impact on such parameters.

METHODS

This was a prospective longitudinal study involving fetuses of women with apparently uncomplicated pregnancies and their newly born babies. Pregnant women attending for routine antenatal care at St. George's Hospital between November 2012 and May 2014 were recruited if the pregnancies were assessed as normal and fetuses had structurally normal hearts. Exclusion criteria were: fetal structural abnormality, impaired fetal growth, any maternal pre-pregnancy or pregnancy-related co-morbidity and pregnant women in labor. All participants gave written consent for fetal and neonatal echocardiogram. The Ethics Committee of NRES Committee London-Surrey Borders approved the study protocol (Reference -12/LO/0945).

Fetal M-mode, two-dimensional (2D) or B-mode, spectral or pulsed wave (PW) Doppler, PW tissue Doppler imaging (TDI) and speckle tracking imaging (STI) echocardiograms were performed few days before birth. Neonatal cardiac assessment was conducted within hours after birth. One investigator (OP) performed all ultrasound examinations using a Toshiba Aplio MX ultrasound system (Toshiba Medical Systems, Japan). Fetal M-mode, B-mode and PW Doppler measurements were made with the convex array transducer PVT-375BT (3.5MHz), whilst the sector paediatric heart probe PST-65AT (6.5MHz) was used for neonatal heart examination. Fetal and neonatal PW-TDI curves and 2D images for STI analysis were obtained and recorded with the multi sector tissue harmonic (TH) transducer PST-30 BT (3MHz) with TDI mode activated. All neonatal examinations were recorded with simultaneous electrocardiogram (ECG). In the absence of a fetal ECG, the cardiac cycle was determined from a dummy ECG device (Lionheart 2 BIO-TEK®Multiparameter Simulator), and mechanical movements of the mitral valve.

M-mode ultrasound was used for assessment of LV shortening fraction (SF) and longitudinal axis ventricular systolic function. *B-mode (2D) imaging* was performed to measure ventricular chamber (RV and LV end-diastolic dimensions (EDD), end-systolic dimensions (ESD), RV/LV EDD ratio,

ventricular end-diastolic and end-systolic areas, and RV and LV sphericity index calculated by dividing ventricular EDD by ventricular end-diastolic length in the apical/basal 4-chamber view), ventricular wall thickness, and valve diameters. *PW Doppler technique* was used to obtain Doppler signals from the inflow and outflow tracts for evaluation of diastolic and systolic function respectively, for calculation of stroke volume and cardiac output (CO), and for estimation of LV myocardial performance index (MPI). *PW-TDI technique* was applied to derive cardiac indices of myocardial motion in systole (S') and diastole (E' and A'), and was also used for estimation of MPI for both right ventricle and left ventricles (MPI'). All echocardiographic measurements were performed according to the standardised protocol of the study and with regards to previously described fetal echo techniques (Supplementary data). For fetal *speckle tracking imaging* care was taken to obtain 2D four-chamber apical or basal images. The narrowest possible ultrasound field and a single focal zone were used during image acquisition to obtain the frame rates *greater than 100 frames per second (fps)*. These settings provided an acceptable combination of high temporal resolution with spatial definition to enhance the feasibility of the frame-by-frame tracking technique. Following the observation of several fetal heart beats, the real-time image was frozen and one cardiac cycle was recorded. With the dummy ECG set at 60bpm, the system was able to capture at least one whole fetal cardiac cycle with real fetal heart rate of 120-150bpm. When several digital clips were obtained, raw data were transferred to a computer for off-line analysis with frame rates greater than 100 fps using a dedicated software (TDI and STI Toshiba software Advanced Cardiac Package, ACP) on a BTO® laptop. The 2D clips were visually inspected and the one with the best endocardial border definition was chosen for STI analysis. The cardiac cycle was defined with M-mode function (M-Graph) incorporated into the Toshiba software whereby an M-mode trace was obtained by placing a cursor line on the 2D image. This provided a guide to set the R wave position. Visualisation of opening (start of the diastole) and closure (start of systole) of atrioventricular valves (AVV) was used to confirm definition of the cardiac cycle. The endocardial and epicardial surfaces of the myocardial segment were manually traced by a point-and-click

approach. When the trace was recognised and accepted by the software, it was then automatically generated by the system by creating a region of interest and providing segmental longitudinal strain and strain rate values, and then generated strain and strain rate curves for each selected myocardial segment. From these curves, the regional and global (by averaging values observed in all 6 segments) peak values were obtained. The peak systolic values of global and segmental longitudinal strain and systolic longitudinal strain rate were recorded for LV and RV separately. All temporal indices (PW-TDI derived time-intervals) were adjusted for heart rate by dividing the values by the cardiac cycle length (all crude values are presented in Supplementary data).

Sample size and power calculations were performed prior to the study based on our pilot data and the previous research study (13). For the systolic strain rate as a primary outcome, a sample of 80 fetuses and 80 neonates would detect a rate of deformational change (1/s) difference of 0.74 (equivalent to 10% of the mean, 3.69), with a power of 85%, a significance level of 5%, and assuming a standard deviation of 1.10. To allow for possible confounding factors including dropouts, this number was increased to 100 fetuses and 100 neonates. Statistical analysis was performed using SPSS version 22.0 (SPSS Inc., Chicago, IL, USA). Both Shapiro-Wilk and Kolmagorov-Smirnov tests were performed to test normality. If $p>0.05$, the data distribution was considered to be normal. For normally distributed data, a paired t-test was used to test the null hypothesis that there was no difference in the means between the fetal and neonatal values. Skewed data was analysed with nonparametric test (Wilcoxon signed rank test). The level of significance was adjusted for multiple measurements. The differences between prenatal and postnatal measurements were deemed as significant only if the p-values less than 0.001 (Bonferroni correction for type 1 error or false positive results of multiple measurements).

B-mode, M-mode, PW Doppler, TDI and STI measurements of 25 fetal and 25 neonatal echoes were repeated by the same observer (OP) on a Toshiba Aplio MX US machine in the same frame

for calculation of the measurement error, and in a different frame for calculation of the overall error (combined acquisition and measurement errors). In randomly chosen 10 fetal and 10 neonatal echocardiograms, two different observers (VDZ and BS) repeated TDI measurements on Toshiba Aplio MX, and STI indices on vendor-specific ACP software in the same frame and then in a different frame. The observers were blinded to each other's measurements. Both, limits of agreement (LoA) with Bland-Altman graphs/Pitman's test of difference in variance, and intra-class correlation coefficient (ICC) were calculated.

RESULTS

A total of 118 women consented to the study. Of these, paired fetal and neonatal data were available for 108 cases. All 108 neonates had a small (≤ 2mm) patent foramen ovale, whereas a small patent ductus arteriosus (≤ 2-3mm) was present in 102 (94%) neonates. After birth, the presence of structurally normal heart was confirmed in all 108 neonates. Demographic characteristics and echocardiographic scan details are summarized in Table 1.

Morphometric measurements by B-mode and M-mode

Morphometric measurements by 2D-dimensional imaging (B-mode) demonstrated a significant decrease in RV EDD, RV/LV EDD ratio, RV AVV dimension, RV/LV AVV dimension ratio, RV/LV end-diastolic area ratio, RV sphericity index and thickness of LV, RV walls and inter-ventricular septum (IVS) (Table 2, Table S1, Figure 1). There was also a significant increase in aortic and pulmonary valve dimension, LV EDD, LV ESD and LV AVV dimension, LV area, both LV and RV end-diastolic length and LV sphericity index (Table 2, Table S1).

Haemodynamic indices

The LV shortening fraction did not differ perinatally. There was evidence of a significant postnatal increase in LV SV and LV CO, whilst RV SV and RV CO decreased significantly after birth with a significant drop in neonatal heart rate (Table 3, Table S2).

Longitudinal axis annular motion changes and MPI changes

There were no significant changes in the RV, LV and IVS longitudinal axis systolic annular motion (Table 3). There was a significant decrease in RV MPI', and LV MPI and MPI' (Tables 3, Table S2, Figure 2).

Myocardial deformation changes by speckle tracking imaging (STI)

The mean frame rate ± SD obtained for STI analysis was *135 ± 14 fps* for fetuses and *128 ± 11 fps* for neonates. The global longitudinal strain rate showed a significant decrease of systolic peak in both ventricles and regional myocardial deformation analysis demonstrated a significant perinatal decrease in longitudinal systolic strain rate in most segments (Table 3, Table S3).

Pulsed waved (PW) Doppler and spectral tissue Doppler imaging (PW-TDI) indices.

There was a significant increase in systolic annular peak velocities (S') for the right ventricle and the inter-ventricular septum but not for the left ventricle (Table 3, Figure 3). There was a significant increase in RV ejection time, and a significant decrease in both RV and LV isovolumetric contraction time (Table 4). Diastolic function indices showed a significant increase in both LV and RV E/A ratio. Similarly, spectral tissue Doppler imaging demonstrated a significant increase in diastolic LV E'/A' ratio, IVS E'/A' ratio and a significant decrease in both LV and RV isovolumetric relaxation time (Table 3, Figure 3).

Reproducibility and repeatability

The limits of agreement (Lo) and intra-class correlation coefficient (ICC) showed good to excellent intra- and inter-observer agreement of all fetal and neonatal conventional, TDI and STI indices in the same frame (ICC=0.8-0.9). When all measurements were repeated in different frame, the correlation and agreement remained excellent to good for both fetal and neonatal conventional and TDI parameters, and showed moderate to good correlation (ICC=0.6-0.7) and good to excellent agreement for fetal and neonatal STI indices (Table S4).

DISCUSSION

The findings of this study in paired human fetuses and neonates provide evidence to support the concept that the perinatal period is associated with significant changes in fetal cardiac geometry, global myocardial performance and ventricular function. The observed changes are most likely explained by cardiac geometrical and functional adaptation in response to the significant alterations in volume and resistance loading conditions both at the end of pregnancy and at birth.

Cardiac Geometry

Only few previous perinatal studies assessed the cardiac chamber geometry at term by means of M-mode with conflicting results (3-6). While some of these studies reported greater RV end-diastolic dimensions compared to LV measurements in term fetus (4, 6), one research group found geometrical ventricular uniformity (3). Our study finding showed RV dominance in term fetuses with the right ventricle being larger and more globular in shape compared to the LV chamber. The right ventricle near term is faced with an increase in preload due to the increasing volume of blood flow to the rapidly growing fetus. Moreover, there is a decrease of the blood shunting across the foramen ovale, as pulmonary blood flow and venous return increase. This was thought could lead to volume loading of the right heart (14, 15). At the same time, the combination of maturational changes in the placenta (15), increased low body vascular resistance (16), and relative restriction of the arterial duct (15) were suggested as possible reasons for an increase in RV afterload.

Experimental sheep studies demonstrated that fetal ventricular function, and RV in particular, is very sensitive to further increases in afterload (17), while increased preload might contribute to the increased cardiomyocyte proliferation, terminal differentiation and enlargement that lead to ventricular dilation and compensatory wall thickening (18). Thus, the increased fetal RV dimension and thickness of the free wall observed in this study would appear to be an adaptive mechanism to cope with the problem of generating sufficient cardiac output, minimizing wall stress and maximizing myocardial perfusion (18). Additionally, cardiomyocyte enlargement was shown to accelerate 10 days before birth and to coincide with the cortisol surge that might suggest a potentially important role of cortisol in the terminal remodeling of the late gestation fetal heart (19). In contrast to the right ventricle, the term fetuses in our study had smaller and less spherical morphology left ventricle that could result from a combination of factors causing low preload to the left heart, namely high pulmonary vascular resistance and extra-cardiac constraint by the liquid-filled lungs, pericardium and thorax (20), and low LV afterload because a progressive decrease in brachiocephalic blood-flow resistance (21). After birth, our study revealed a reduction in RV end-diastolic diameter and an increase in RV length resulting in a significant perinatal decrease in RV sphericity index, reflecting a less globular RV shape. These immediate postnatal changes could be attributed to the fact that RV volume preload fall due to elimination of the placental circulation, while the RV afterload decreased as a consequence of a drop in pulmonary vascular resistance with lung aeration. In contrast, there was a perinatal expansion of LV chamber with a significant increase in both LV end-diastolic dimension and LV length. As a result of predominantly increased LV end-diastolic dimensions, LV sphericity index increased signifying a more globular LV chamber. The observed postnatal changes in LV geometry could be explained by combination of factors: a considerable increase in LV volume load due to an increased pulmonary venous return, an increase in LV resistance load as a result of a rise in systemic vascular resistance, and a decrease of the pericardial constraint. Greater preload and afterload leading to greater LV and RV sphericity was recently observed in different fetal (22-24) and neonatal (25) pathological conditions.

Cardiac function

Global myocardial performance

The data on perinatal changes in MPI index are scant and discordant (8-10, 26). A raised MPI is a sensitive and non-specific marker of fetal cardiac dysfunction in different pathological fetal conditions but is a load-dependent index (27). Our study demonstrates a significant postnatal decrease in MPI in both ventricles at the expense of decreased IVC and IVR time intervals in both ventricles and an increased RV ejection time. This finding may be explained by acute changes in loading conditions in both ventricles, as adjusting these time intervals by cardiac cycle length eliminated the effect of heart rate. Perinatal MPI trends found in our study were congruent with previous studies for the LV (26) and RV (8, 10, 26).

Haemodynamics

LV shortening fraction (SF) did not show any change from fetus to neonate that was in keeping with our results of significant perinatal increase in both LV end-diastolic and end-systolic dimensions. This was in disagreement to the previous early M-mode study that found perinatal increase in LVSF in the first hours of life (5). The discrepancies could be due to the lower recruitment (n=34) in the latter study, and the fact that the fetal assessment was performed at 12-24 hours before delivery as opposed to 8 days before birth in our study.

Our results also showed evidence of fetal RV cardiac output dominance as previously reported (28, 29). Postnatally, LV CO significantly increased resulting in LV CO predominance. Our findings revealed that with a dramatic fall in heart rate, a significant rise in LV CO was due to a perinatal increase in LV stroke volume associated with an increased LV preload and greater LV dimensions, whereas a significantly decreased RV CO might reflect a reduced RV preload. The overall ventricular size is an important determinant of stroke volume (30), but heart rate is the most effective way for the fetus to increase cardiac output (31, 32). Based on early studies in lambs, neonates are also more dependent on heart rate than stroke volume to change cardiac output (17,

33). In contrast, Doppler studies in humans have demonstrated that newborns can significantly increase the cardiac output without a significant change in heart rate (34), and that the major regulator of LV output immediately after birth is stroke volume and not heart rate (5) – consistent with our findings. Additionally, the presence of a modest shunt across the patent ductus arteriosus in majority of newborns in our study could also contribute to the augmentation of LV stroke volume in the first hours after birth (35).

Systolic function

In our study, the LV and RV global longitudinal strain did not show any perinatal change that was also concordant with unchanged global systolic longitudinal LV and RV annular motion. In contrast, there was a significant reduction in both LV and RV global and regional longitudinal strain rate. Deformational parameters are not only a measure of intrinsic myocardial contractility but are also influenced by changes in cardiac load, structure and heart rate (36), while systolic strain rate appeared to be is a more robust measure of contractility that is less affected by the heart rate (37). Experimental human studies altering LV loading conditions have shown that an acute increase in LV preload and afterload resulted in decreased longitudinal strain rate (38), while RV longitudinal myocardial deformational parameters demonstrated reduction under conditions of an abrupt decrease in volume loading (39). Our findings are in agreement with these experimental data, and showed that a significant fall in the rate of longitudinal deformation of both ventricles could be attributed to acute changes in hemodynamic load with decreased RV and increased LV preload and afterload in the transition from intra- to extra-uterine life. Decreased postnatal longitudinal deformational rate occurring under different loading conditions may reflect ventricular morphological and physiological differences. LV myocardial architecture comprises of three layers of muscle fibers with predominantly radial and circumferential thickening with additional rotational and twisting motion and is designed to act as a high-resistance, high “pressure pump”, whereas right ventricle has a predominant longitudinal myocyte orientation and functions as a low-resistance,

low-capacitance "volume pump" (40). This hypothesis is supported by findings of inter-ventricular differences in the expression of genes involved in the response to pressure loading (41), LV and RV divergences in perinatal cardiomyocyte growth trajectories (42), and animal studies demonstrating different responses to inotropic stimulation in left versus right myocardium (43). In accord with our study findings, other recent publications have also shown a decrease in RV (8) and LV (8, 10) longitudinal strain rate from fetus to neonate, albeit not as close to the birth event as our study demonstrated, that could explain the discrepancy of RV perinatal strain rate trend reported by one study where neonatal assessment was conducted at 4-8 weeks after birth (10).

Furthermore, our findings revealed evidence of a postnatal significant increase in RV and IVS systolic myocardial velocities. The impact of loading conditions on myocardial velocities was shown previously (44). Our results could reflect the postnatal acute decrease in RV haemodynamic load with a significant alteration in RV geometry resulting in elevated contractility of RV and IVS basal segments that was in agreement with previous perinatal study (8). Adult studies also found that the right ventricle exhibits remarkable plasticity in its ability to geometrical and functional recovery after being "unloaded" in cases of RV volume overload (45). It is interesting to speculate that origin of the unique peculiarities of RV plasticity could lie in fetal life. Unchanged values of LV myocardial longitudinal systolic velocities S' might suggest unique LV mechanics of myocardial adaptation with a possible postnatal increase in radial and rotational deformation while reducing the longitudinal global motion. Hitherto, the perinatal data on changes in systolic myocardial velocities are very limited and inconsistent (8, 9). Our findings were in agreement with one study (8), and in contrast with another research group that found a decrease in systolic myocardial velocities of both ventricles during the transition from fetus to neonate (9). The contradictory findings in the latter study could be explained by the use of two different ultrasound platforms, the relatively small number of normal infants studied (n=37) and inclusion of pathological pregnancies.

Diastolic function

Our results demonstrated that LV and RV spectral Doppler inflow pattern in term fetuses had a small E-wave, a dominant A-wave with E/A ratio <1 consistent with previously reported AVV inflow pattern in term fetus (7, 46). After birth, in agreement with previous studies, LV E/A (7, 46) and LV E'/A' (8, 9) ratios were >1; there was also a significant increase in RV E/A (8, 9) and IVS E'/A' ratios (9). Our perinatal changes in LV ventricular filling pattern could be explained by combination of the several factors: spontaneous ventilation after birth resulting in decreased pericardial pressure, which facilitate greater pulmonary blood flow and therefore the sharp increase in left atrial venous return (47), the greater LV preload , and the slower heart rate that could contribute to the augmentation the early or passive diastolic filling. Both reduced pericardial constrain and decrease heart rate could facilitate the improvement of the RV diastolic properties postnatally.

Moreover, low E/A ratio was previously reported as an indicator of poor compliance. Current data on fetal myocardial compliance as a determinant of myocardial relaxation is conflicting. There was an accepted opinion that fetal myocardium is less compliant that negatively affects myocardial performance. Recent data has proposed that fetal myocardial compliance is much higher than in the postnatal heart, and that this is predominantly due to the differences in the expression of particular isoform of titin (48, 49). Animal fetal hearts were shown to express exclusively a unique N2BA subtype, which is rapidly disappeared at birth and replaced by a smaller N2B isoform resulting in an increase in stiffness of the postnatal heart in the first days after birth. Increase in stiffness postnatally could have a protective role by limiting the cardiac extensibility to balance the reduced extra-cardiac constraint (49). Furthermore, increase in titin elastic recoil is thought to also contribute to myocardial contractility augmentation (49), thus adjusting to the intensified pump function of the postnatal heart. Moreover, it was previously shown that the immature fetal myocardium have reduced inherent contractility and contractile reserve due to increased non-contractile elements, impaired calcium uptake, myocardial cellular replication by hyperplasia rather

than hypertrophy and decreased sympathetic innervation with glycolysis and lactate oxidation being the major sources of energy store (50). Recent findings in the murine model (51) and human data (52) suggest that neonatal myocardium exhibit unique regenerative intrinsic myocardial properties in the first few days after birth. Profound alteration in loading conditions accompanied by a rapid perinatal shift in cardiomyocyte metabolism from carbohydrate to fatty acid utilization, perinatal increase in cortisol level and maturation of the thyroid axis may help facilitate cardiac adaptation and cardiomyocyte maturation.

Strength and limitations

The main strength of the present study was its prospective design and the inclusion of a healthy study population where the impact of birth - a natural intervention - was studied longitudinally. One of the limitations of our study was that the Toshiba software tended to produce consistently lower deformational indices than reported previously. However, to date, there have not been any published fetal or neonatal STI studies conducted on the same platform, and a great variation in fetal deformational parameter values on different vendors has still remained unresolved issue. Considering that the raw data in our study were obtained at very high frame rates (>100 fps) and transferred to the software without compression, any temporal undersampling resulting in underestimation of STI values could be excluded. Additionally, as in all fetal STI studies, both dummy ECG and mitral valve motion were used to define heart cycles that was done accurately in this study, but still was an approximation to the ECG used in neonates.

Conclusions

The findings of this study demonstrate significant perinatal change in ventricular geometry, myocardial performance and cardiac function from fetus to neonate consistent with the profound alterations in volume and resistance load associated with circulatory and maturational adaptation at birth. Improved knowledge of the geometrical and functional parameters of the fetal heart at term

and the alterations occurring after birth could help understanding and interpretation of the perinatal adaptation mechanisms in normal pregnancies and alteration of these processes in compromised fetal and neonatal conditions.

SUPPLEMENTARY DATA

Supplementary data include a detailed description of all study methods and supplemental tables.

ACKNOWLEGEMENTS

We are grateful to all patients taken part in this study for their great enthusiasm they showed and the trust they placed in us. We also thank Toshiba Ultrasound Company for providing US platform and software for this research, Miss Vahideh Davatgar Zahiri and Mr Benjamin Smith for helping with echo measurements for inter-observer reproducibility study, and all sonographers, midwives and doctors of the Fetal Medicine Unit, St. George's Hospital for their contribution to the patient's recruitment.

FUNDING SOURCES

OP was partly supported by Children's Heart Unit Fund (CHUF), Royal Brompton and Harefield Hospital Charity [registration number 1053584].

CONFLICT OF INTERESTS

None declared.

REFERENCES

1. Fouron JC. The unrecognized physiological and clinical significance of the fetal aortic isthmus. *Ultrasound Obstet Gynecol*. 2003;22:441-7.

2. Rudolph AM. Distribution and regulation of blood flow in the fetal and neonatal lamb. *Circ Res*. 1985;57:811-21.

3. Wladimiroff JW, Vosters R, McGhie JS. Normal cardiac ventricular geometry and function during the last trimester of pregnancy and early neonatal period. *Br J Obstet Gynaecol*. 1982;89:839-44.

4. Azancot A, Caudell TP, Allen HD, Horowitz S, Sahn DJ, Stoll C, et al. Analysis of ventricular shape by echocardiography in normal fetuses, newborns, and infants. *Circulation*. 1983;68:1201-11.

5. Agata Y, Hiraishi S, Oguchi K, Misawa H, Horiguchi Y, Fujino N, et al. Changes in left ventricular output from fetal to early neonatal life. *J Pediatr*. 1991;119:441-5.

6. Veille JC, Hanson R, Steele L, Tatum K. M-mode echocardiographic evaluation of fetal and infant hearts: longitudinal follow-up study from intrauterine life to year one. *Am J Obstet Gynecol*. 1996;175:922-8.

7. Kim HW, Lee HY, Baik SJ, Hong YM. Atrioventricular Flow Wave Patterns before and after Birth by Fetal Echocardiography. *J Cardiovasc Ultrasound*. 2012;20:85-9.

8. Schubert U, Muller M, Norman M, Abdul-Khaliq H. Transition from fetal to neonatal life: Changes in cardiac function assessed by speckle-tracking echocardiography. *Early Hum Dev*. 2013.

9. Iwashima S, Sekii K, Ishikawa T, Itou H. Serial change in myocardial tissue Doppler imaging from fetus to neonate. *Early Hum Dev*. 2013;89:687-92.

10. Maskatia SA, Pignatelli RH, Ayres NA, Altman CA, Sangi-Haghpeykar H, Lee W. Longitudinal Changes and Interobserver Variability of Systolic Myocardial Deformation Values in a Prospective Cohort of Healthy Fetuses across Gestation and after Delivery. *J Am Soc Echocardiogr*. 2016.

11. Cabrera AG, Chen DW, Pignatelli RH, Khan MS, Jeewa A, Mery CM, et al. Outcomes of anomalous left coronary artery from pulmonary artery repair: beyond normal function. *Ann Thorac Surg*. 2015;99:1342-7.

12. Tham EB, Smallhorn JF, Kaneko S, Valiani S, Myers KA, Colen TM, et al. Insights into the evolution of myocardial dysfunction in the functionally single right ventricle between staged palliations using speckle-tracking echocardiography. *J Am Soc Echocardiogr*. 2014;27:314-22.

13. Willruth AM, Geipel AK, Fimmers R, Gembruch UG. Assessment of right ventricular global and regional longitudinal peak systolic strain, strain rate and velocity in healthy fetuses and impact of gestational age using a novel speckle/feature-tracking based algorithm. *Ultrasound Obstet Gynecol*. 2011;37:143-9.

14. Baschat AA. The fetal circulation and essential organs-a new twist to an old tale. *Ultrasound Obstet Gynecol*. 2006;27:349-54.

15. Gardiner HM. Response of the fetal heart to changes in load: from hyperplasia to heart failure. *Heart*. 2005;91:871-3.

16. Mari G. Arterial blood flow velocity waveforms of the pelvis and lower extremities in normal and growth-retarded fetuses. *Am J Obstet Gynecol*. 1991;165:143-51.

17. Gilbert RD. Effects of afterload and baroreceptors on cardiac function in fetal sheep. *J Dev Physiol*. 1982;4:299-309.

18. Jonker SS, Giraud MK, Giraud GD, Chattergoon NN, Louey S, Davis LE, et al. Cardiomyocyte enlargement, proliferation and maturation during chronic fetal anaemia in sheep. *Exp Physiol*. 2010;95:131-9.

19. Feng X, Reini SA, Richards E, Wood CE, Keller-Wood M. Cortisol stimulates proliferation and apoptosis in the late gestation fetal heart: differential effects of mineralocorticoid and glucocorticoid receptors. *Am J Physiol Regul Integr Comp Physiol*. 2013;305:R343-50.

20. Grant DA, Fauchere JC, Eede KJ, Tyberg JV, Walker AM. Left ventricular stroke volume in the fetal sheep is limited by extracardiac constraint and arterial pressure. *J Physiol*. 2001;535:231-9.

21. Rudolph AM, Heymann MA. Circulatory changes during growth in the fetal lamb. *Circ Res*. 1970;26:289-99.

22. Crispi F, Bijnens B, Figueras F, Bartrons J, Eixarch E, Le Noble F, et al. Fetal growth restriction results in remodeled and less efficient hearts in children. *Circulation*. 2010;121:2427-36.

23. Brooks PA, Khoo NS, Mackie AS, Hornberger LK. Right ventricular function in fetal hypoplastic left heart syndrome. *J Am Soc Echocardiogr*. 2012;25:1068-74.

24. Brooks PA, Khoo NS, Hornberger LK. Systolic and diastolic function of the fetal single left ventricle. *J Am Soc Echocardiogr*. 2014;27:972-7.

25. Rodriguez-Lopez M, Osorio L, Acosta-Rojas R, Figueras J, Cruz-Lemini M, Figueras F, et al. Influence of breastfeeding and postnatal nutrition on cardiovascular remodeling induced by fetal growth restriction. *Pediatr Res*. 2016;79:100-6.

26. Tsutsumi T, Ishii M, Eto G, Hota M, Kato H. Serial evaluation for myocardial performance in fetuses and neonates using a new Doppler index. *Pediatr Int*. 1999;41:722-7.

27. Uemura K, Kawada T, Zheng C, Li M, Shishido T, Sugimachi M. Myocardial performance index is sensitive to changes in cardiac contractility, but is also affected by vascular load condition. *Conf Proc IEEE Eng Med Biol Soc*. 2013;2013:695-8.

28. Mielke G, Benda N. Cardiac output and central distribution of blood flow in the human fetus. *Circulation*. 2001;103:1662-8.

29. Prsa M, Sun L, van Amerom J, Yoo SJ, Grosse-Wortmann L, Jaeggi E, et al. Reference ranges of blood flow in the major vessels of the normal human fetal circulation at term by phase-contrast magnetic resonance imaging. *Circ Cardiovasc Imaging*. 2014;7:663-70.

30. Marciniak A, Claus P, Sutherland GR, Marciniak M, Karu T, Baltabaeva A, et al. Changes in systolic left ventricular function in isolated mitral regurgitation. A strain rate imaging study. *Eur Heart J*. 2007;28:2627-36.

31. Noori S, Stavroudis TA, Seri I. Systemic and cerebral hemodynamics during the transitional period after premature birth. *Clin Perinatol*. 2009;36:723-36, v.

32. Piot C, LeMaire SA, Albat B, Seguin J, Nargeot J, Richard S. High frequency-induced upregulation of human cardiac calcium currents. *Circulation*. 1996;93:120-8.

33. Davidson D. Circulating vasoactive substances and hemodynamic adjustments at birth in lambs. *J Appl Physiol (1985)*. 1987;63:676-84.

34. Gullberg N, Winberg P, Sellden H. Changes in stroke volume cause change in cardiac output in neonates and infants when mean airway pressure is altered. *Acta Anaesthesiol Scand*. 1999;43:999-1004.

35. Drayton MR, Skidmore R. Ductus arteriosus blood flow during first 48 hours of life. *Arch Dis Child*. 1987;62:1030-4.

36. Boettler P, Hartmann M, Watzl K, Maroula E, Schulte-Moenting J, Knirsch W, et al. Heart rate effects on strain and strain rate in healthy children. *J Am Soc Echocardiogr*. 2005;18:1121-30.

37. Weidemann F, Jamal F, Sutherland GR, Claus P, Kowalski M, Hatle L, et al. Myocardial function defined by strain rate and strain during alterations in inotropic states and heart rate. *Am J Physiol Heart Circ Physiol*. 2002;283:H792-9.

38. Burns AT, La Gerche A, D'Hooge J, MacIsaac AI, Prior DL. Left ventricular strain and strain rate: characterization of the effect of load in human subjects. *Eur J Echocardiogr*. 2010;11:283-9.

39. Ko HK, Yu JJ, Cho EK, Kang SY, Seo CD, Baek JS, et al. Segmental Analysis of Right Ventricular Longitudinal Deformation in Children before and after Percutaneous Closure of Atrial Septal Defect. *J Cardiovasc Ultrasound*. 2014;22:182-8.

40. Friedberg MK, Redington AN. Right versus left ventricular failure: differences, similarities, and interactions. *Circulation*. 2014;129:1033-44.

41. Bogaard HJ, Abe K, Vonk Noordegraaf A, Voelkel NF. The right ventricle under pressure: cellular and molecular mechanisms of right-heart failure in pulmonary hypertension. *Chest*. 2009;135:794-804.

42. Jonker SS, Louey S. Endocrine and other physiologic modulators of perinatal cardiomyocyte endowment. *J Endocrinol*. 2016;228:R1-18.

43. Molina CE, Johnson DM, Mehel H, Spatjens RL, Mika D, Algalarrondo V, et al. Interventricular differences in beta-adrenergic responses in the canine heart: role of phosphodiesterases. *J Am Heart Assoc*. 2014;3:e000858.

44. Bauer F, Jamal F, Douillet R, Le Roi F, Bouchoule I, Bizet-Nafeh C, et al. [Acute changes in load: effects of myocardial velocities measured by doppler tissue imaging]. *Arch Mal Coeur Vaiss*. 2001;94:1155-60.

45. Brittain EL, Hemnes AR, Keebler M, Lawson M, Byrd BF, 3rd, Disalvo T. Right ventricular plasticity and functional imaging. *Pulm Circ*. 2012;2:309-26.

46. Veille JC, Smith N, Zaccaro D. Ventricular filling patterns of the right and left ventricles in normally grown fetuses: a longitudinal follow-up study from early intrauterine life to age 1 year. *Am J Obstet Gynecol*. 1999;180:849-58.

47. Grant DA, Kondo CS, Maloney JE, Walker AM, Tyberg JV. Changes in pericardial pressure during the perinatal period. *Circulation*. 1992;86:1615-21.

48. Walker JS, de Tombe PP. Titin and the developing heart. *Circ Res*. 2004;94:860-2.

49. Opitz CA, Leake MC, Makarenko I, Benes V, Linke WA. Developmentally regulated switching of titin size alters myofibrillar stiffness in the perinatal heart. *Circ Res*. 2004;94:967-75.

50. Finnemore A, Groves A. Physiology of the fetal and transitional circulation. *Semin Fetal Neonatal Med*. 2015;20:210-6.

51. Porrello ER, Mahmoud AI, Simpson E, Hill JA, Richardson JA, Olson EN, et al. Transient regenerative potential of the neonatal mouse heart. *Science*. 2011;331:1078-80.

52. Haubner BJ, Schneider J, Schweigmann U, Schuetz T, Dichtl W, Velik-Salchner C, et al. Functional Recovery of a Human Neonatal Heart After Severe Myocardial Infarction. *Circ Res*. 2016;118:216-21.

Table 1. Demographic characteristic of the study population

Parameter	Characteristics
Maternal characteristics (n=108)	
Maternal age (years)	34 ± 5
Ethnicity (number):	
Caucasian	80 (74%)
Asian	21 (19%)
Afro-Caribbean	7 (7%)
Fetal cardiac assessment (n=108)	
Gestational age (weeks)	39 ±1.5
Time gap between the fetal scan and birth (days)	8 (10)
Neonatal cardiac assessment (n=108)	
Neonate's age at the time of scan (hours)	13 (16)
Neonate's sex male (number)	58 (54%)
Neonate's weight (kg)	3.51 ± 0.47

Values are mean ±SD, median (interquartile range), or n (%).

Table 2. Perinatal changes in cardiac geometry

Measurements	Fetal	Neonatal	P
RV sphericity index*	0.53 ± 0.09	0.40 ± 0.05	<0.0001
LV sphericity index*	0.46 ± 0.09	0.49 ± 0.05	0.001
RV/LV end-diastolic area ratio	1.10 (0.37)	0.80 (0.20)	<0.0001
RV/LV atrio-ventricular valve dimension ratio	1.16 (0.20)	1.02 (0.18)	<0.0001
RV wall thickness, mm	3.8 (0.8)	3.2 (0.9)	<0.0001
LV wall thickness, mm	3.7 (0.8)	3.2 (0.5)	<0.0001
IVS thickness, mm	3.6 ± 0.6	3.2 ± 0.6	<0.0001

Data are mean ± SD, median (interquartile range). Sphericity index*, the cardiac index calculated by dividing ventricular end-diastolic dimension by ventricular end-diastolic length measured in the apical/basal 4-chamber view.

Table 3. Perinatal changes in indices of cardiac function

Measurements	Fetal	Neonatal	P
Haemodynamics			
Heart rate, bpm	140 (13)	117 (16)	<0.0001
LV cardiac output, ml/min/kg	212 ± 55	275 ± 65	<0.0001
RV cardiac output, ml/min/kg	279 ± 77	211 ± 54	<0.0001
Global myocardial performance			
LV MPI'	0.60 (0.21)	0.47 (0.10)	<0.0001
RV MPI'	0.61 ± 0.14	0.42 ± 0.08	<0.0001
Systolic function			
LV longitudinal axis motion, mm	7.1 (1.7)	6.6 (1.5)	0.020
IVS longitudinal axis motion, mm	5.8 (1.7)	5.4 (1.4)	0.074
RV longitudinal axis motion, mm	8.7 (2.8)	9.0 (2.2)	0.125
LV global longitudinal systolic strain rate, 1/s	-1.4 (0.9)	-1.0 (0.4)	<0.0001
RV global longitudinal systolic strain rate, 1/s	-1.5 (0.7)	-1.0 (0.6)	<0.0001
LV S', cm/s	5.2 ± 1.4	5.1 ± 0.8	0.473
LV ejection time', s*	0.37 ± 0.05	0.39 ± 0.05	0.017
LV isovolumetric contraction time', s*	0.12 ± 0.02	0.09 ± 0.02	<0.0001
RV ejection time', s*	0.39 ± 0.05	0.41 ± 0.05	<0.0001
RV isovolumetric contraction time', s*	0.11 (0.054)	0.08 (0.03)	<0.0001
Diastolic function			
LV E/A ratio	0.8 (0.2)	1.2 (0.3)	<0.0001
RV E/A ratio	0.7 (0.2)	0.9 (0.4)	<0.0001
LV E'/A' ratio	0.8 (0.5)	1.1 (0.5)	<0.0001
IVS E'/A' ratio	0.7 (0.3)	0.8 (0.4)	<0.0001

RV E/E' ratio	7.7 (3.8)	6.4 (3.0)	0.023
LV isovolumetric relaxation time', s*	0.11 (0.03)	0.09 (0.02)	<0.0001
RV isovolumetric relaxation time', s*	0.11 (0.04)	0.09 (0.02)	<0.0001

Data are mean ± SD, or median (interquartile range). MPI', myocardial performance index obtained by PW-TDI; E, passive early diastolic velocity obtained by PW Doppler; A, atrial contraction diastolic velocity obtained by PW Doppler; S', systolic annular peak velocity by PW-TDI; E', early diastolic annular velocity by PW-TDI; A', atrial contraction diastolic annular peak velocity by PW-TDI; s, seconds; *, values adjusted by cardiac cycle length.

FIIGURE LEGENDS

Figure 1 Perinatal changes in cardiac chamber geometry.

Linear plots of all 108 patients showing a significant ($p<0.0001$) decrease in (A) RV/LV end-diastolic dimension (EDD) ratio and (B) RV sphericity index from fetus to neonate.

Figure 2 Perinatal changes in myocardial performance index.

Box-and-whisker plots demonstrating a significant ($p<0.0001$) perinatal decrease in LV and RV myocardial performance index (MPI') obtained by PW- tissue Doppler imaging in fetus and neonate.

Figure 3 Perinatal changes in cardiac systolic and diastolic function.

PW- tissue Doppler imaging derived RV systolic (S') and diastolic (E' and A') myocardial velocity measurements in (A) fetus and (B) neonate. Box-and-whisker plots showing a significant ($p<0.0001$) perinatal increase in (C) RV and IVS systolic myocardial velocities S' and (D) LV and IVS diastolic myocardial velocity ratio E'/A' form fetus to neonate.

Figure 1.

Click here to download high resolution image

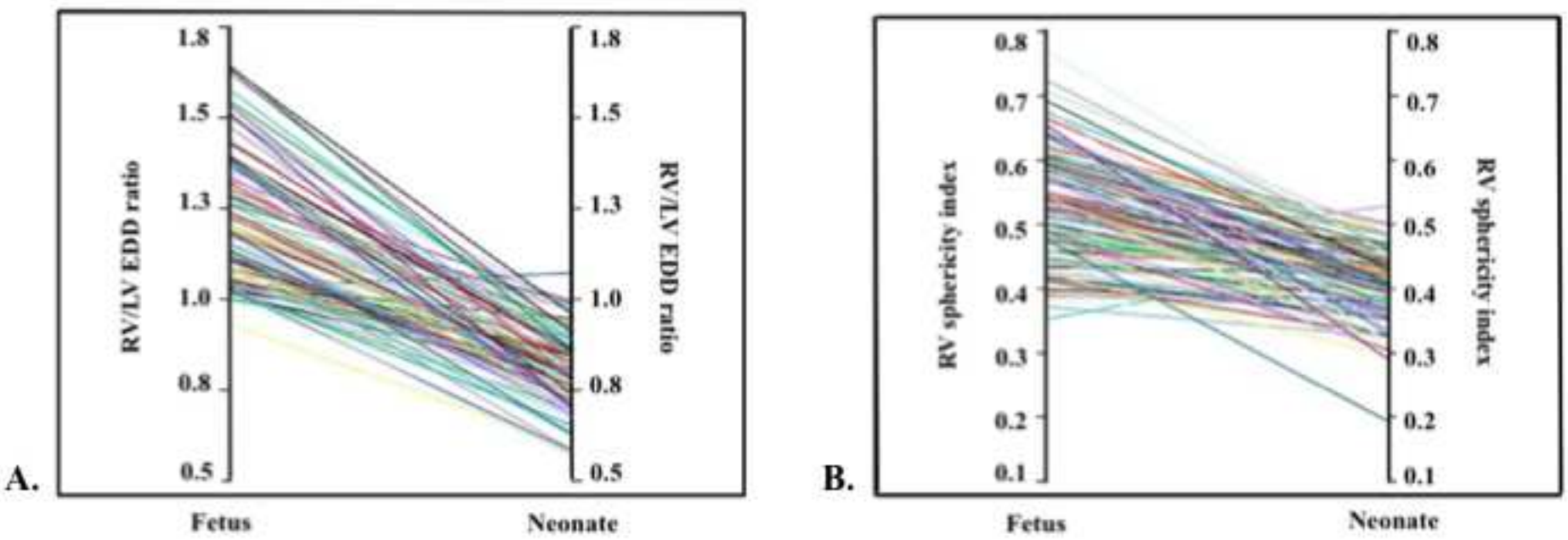

Figure 2.
Click here to download high resolution image

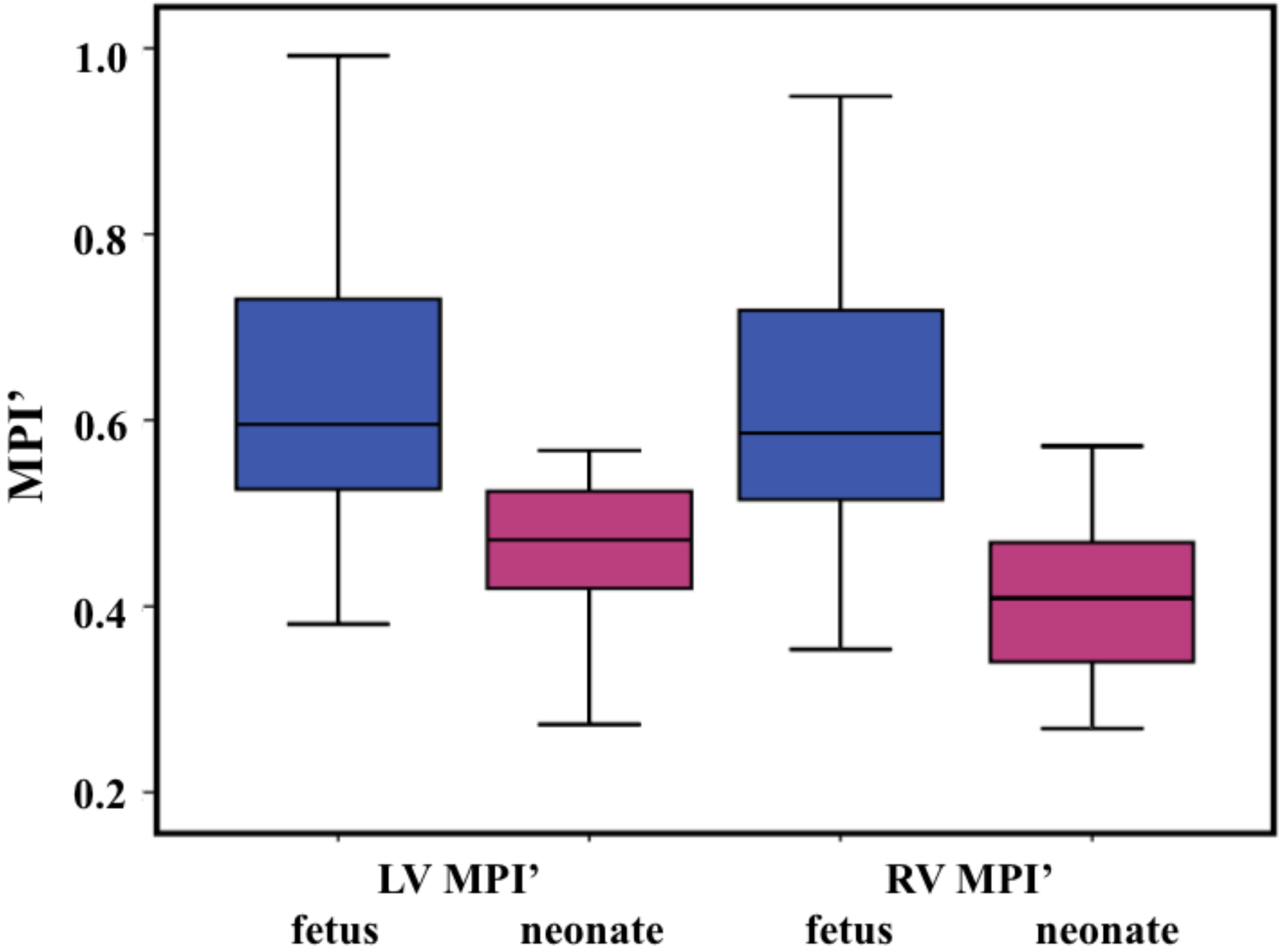

Figure 3.
Click here to download high resolution image

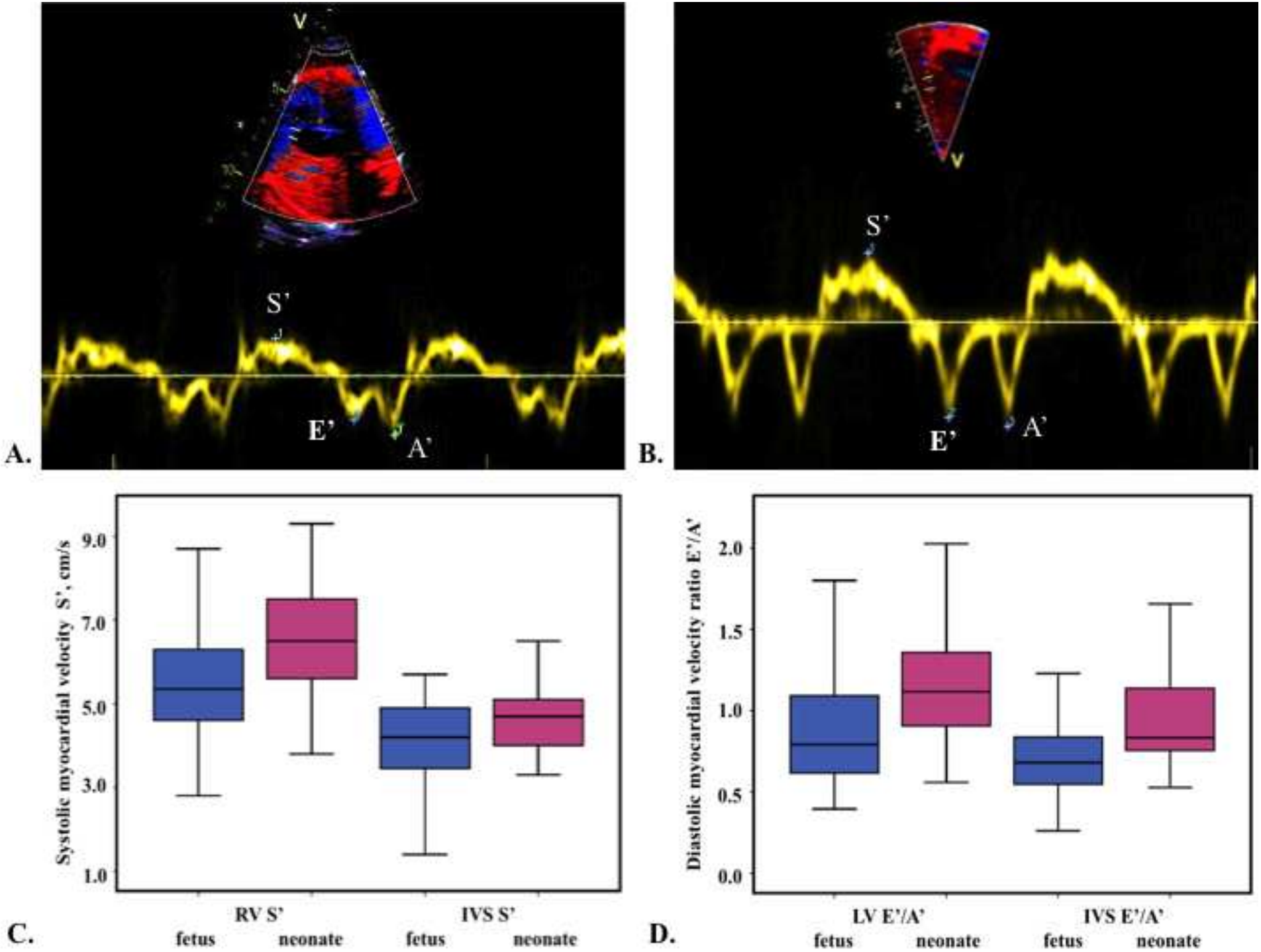

PERINATAL CHANGES IN FETAL VENTRICULAR GEOMETRY, MYOCARDIAL PERFORMANCE AND CARDIAC FUNCTION IN NORMAL TERM PREGNANCIES

SUPPLEMENTARY MATERIAL

- **STUDY METHODS**

1. M-mode technique
2. B-mode (2D imaging)
3. PW Doppler technique
4. PW Tissue Doppler imaging (TDI) technique

- **SUPPLEMENTARY TABLES**

- **SUPPLEMENTRY REFERENCES**

STUDY METHODS

1. M-mode technique

M-mode technique was used for assessment of cardiac geometry and function (RV and LV end-diastolic dimensions (EDD), RV and LV end-systolic dimensions (ESD), ventricular wall thickness, LV/RV EDD ratio and LV shortening fraction (SF)) from four-chamber or short axis views depending on fetal position with M-mode cursor positioned perpendicular to the inter-ventricular septum and just below the atrio-ventricular valves (AVV) (1-3). LV shortening fraction was automatically calculated by ultrasound machine cardiac package utilizing the Teichholz method: SF = (LV EDD – LV ESD/ LV EDD).

Conventional M-mode was also used to assess tricuspid and mitral valve ring movement in relation to the cardiac apex as measurement of ventricular long-axis function. RV, LV and inter-ventricular septum (IVS) longitudinal axis annular excursions were obtained on the echo machine during the scan in fetal apical or basal four chamber view with the M-mode cursor line positioned from cardiac apex to tricuspid and mitral valve annular rings and IVS annular level as previously described (4).

2. B-mode (2D imaging)

B-mode or two-dimensional (2D) imaging with cine loop function facilitated measurements of ventricular chambers (LV and RV EDD at the basal level of the four chamber view, LV and RV end-diastolic ventricular areas by tracing ventricular endocardial borders (5) and valve diameters (1).The sphericity index of both ventricles was calculated as EDD divided by base-to-apex end-diastolic ventricular length (6).

3. PW Doppler technique

Two peaks of the waveform profile were obtained (peak E-early diastolic filling and peak A-atrial contraction) according to the previously published methodology (7), which reflected diastolic function of the respective ventricles. E/A ratio, MV and TV velocity time integrals (VTI) and deceleration time were measured as previously described (8, 9). Ventricular systolic function was derived from outflow tract Doppler examination using aortic and pulmonary valves maximum peak velocity and velocity time integral (VTI) with regards to previously published technique (7).

PW Doppler-valve area method was applied for estimation of both LV and RV stroke volume (SV) and cardiac output (CO). The measurement of LV and RV outflow tract dimensions were obtained according to previously described methodology (7). Assuming a circular shape of the outflow tracts, the cross-sectional area (CSA) of the vessels was calculated as: CSA=0.785 x (D)sq., where D indicated a valve diameter. The stroke volume was calculated as a product of VTI multiplied by CSA of the outflow tract: SV = CSA x VTI. Cardiac output for LV and RV was estimated applying standard equations: CO = SV x HR and normalized by the fetal/neonatal body weight.

PW Doppler technique was also applied for estimation of LV myocardial performance index as a marker of global systolic and diastolic function. The true apical or basal four-chamber view of the heart was obtained, with sample volume positioned between mitral and aortic valves and gate wide enough (3-4mm) to allow simultaneous recording of inflow and outflow profiles. Measurements were performed with regards to the recently proposed stringent criteria for modified MPI (Mod-MPI) image acquisition (10, 11). As an addition to the proposed stringent Mod-MPI technique, not only the apical chamber view but also either basal or apical chamber view was used for image acquisition and subsequent MPI calculation. E/A spectral waveforms were visualized as positive in the apical chamber view, or as negative ones in the basal chamber view. The time cursor was placed at the beginning of valve clicks 'leaning against' but not covering any part of the clicks (10, 12, 13). Four time-intervals were measured in the LV: ejection time (ET), isovolumetric relaxation time (IVRT), relaxation time (RT), and isovolumetric contraction time (IVCT) as previously descreibed (13). MPI was calculated as follows: (IVCT+IVRT)/ET.

4. PW Tissue Doppler imaging technique

PW-TDI was performed in four-chamber view in real time according to previously published methodology (4, 14). Annular peak velocity profiles and their peak values for both right and left ventricles were obtained in systole (S'), early diastole (E'), and atrial contraction (A'). E'/A' and E/E' indices were calculated. LV and RV myocardial performance index (MPI') was calculated by measuring isovolumetric contraction time interval (IVCT'), ejection time (ET') and isovolumetric relaxation time (IVRT') using equation: MPI'=(IVCT'+IVRT')/ET'. All MPI' intervals were measured from the same cardiac cycle (15). Sweep speed, gain and wall motion filter (WMF) optimized in the same way as for PW Doppler Mod-MPI technique (10, 11).

SUPPLEMENTARY TABLES

Table S1. Perinatal changes in ventricular geometry

Measurements	Fetal	Neonatal	P
RV end-diastolic dimension, mm	16.7 ± 2.0	13.7 ± 1.8	<0.0001
LV end-diastolic dimension, mm	13.9 ± 1.9	16.9 ± 1.7	<0.0001
LV end-systolic dimension, mm	8.86 ± 2.15	11.19 ± 1.78	<0.0001
RV/LV end-diastolic dimension ratio	1.19 (0.26)	0.81 (0.15)	<0.0001
RV end-diastolic length, mm	32.3 (6.5)	34.3 (3.8)	0.001
LV end-diastolic length, mm	31.1 (6.7)	34.6 (3.1)	<0.0001
RV end-diastolic area, mm sq.	3.5 (1.1)	3.5 (1.0)	0.774
LV end-diastolic area, mm sq.	3.2 ± 0.8	4.3 ± 0.8	<0.0001
RV/LV end-diastolic area ratio	1.10 (0.37)	0.80 (0.20)	<0.0001
RV atrio-ventricular valve diameter, mm	11.3 (1.6)	10.4 (1.8)	<0.0001
LV atrio-ventricular valve diameter, mm	9.7 ± 1.2	10.2 ± 1.1	<0.0001
RV/LV atrio-ventricular valve diameter ratio	1.16 (0.20)	1.02 (0.18)	<0.0001
Pulmonary valve diameter, mm	9.0 (1.2)	9.2 (0.8)	0.001
Aortic valve diameter, mm	7.9 (0.9)	8.4 (0.8)	<0.0001
Pulmonary valve /Aortic valve diameter ratio	1.11 (0.12)	1.09 (0.10)	0.006
RV wall thickness	3.80 (0.75)	3.20 (0.85)	<0.0001
LV wall thickness	3.70 (0.80)	3.20 (0.50)	<0.0001
IVS thickness	3.58 ± 0.64	3.22 ± 0.64	<0.0001

Data are mean ± SD, or median (interquartile range). RV, right ventricular; LV, left ventricular; IVS, inter-ventricular septum; Sphericity index*, the cardiac index calculated by dividing ventricular end-diastolic dimension by ventricular end-diastolic length measured in the apical/basal 4-chamber view.

Table S2. Perinatal changes in cardiac function (with crude values)

Measurements	Fetal	Neonatal	P
Haemodynamics			
Heart rate, bpm	140 (13)	117 (16)	<0.0001
Cardiac cycle length, ms	429 (40)	513 (70)	<0.0001
LV shortening fraction, %	35.5 ± 3.1	35.0 ± 3.5	0.610
LV stroke volume, ml/beat	5.3 ± 1.4	8.1 ± 2.4	<0.0001
RV stroke volume, ml/beat	7.0 ± 2.0	6.3 ± 1.6	<0.001
Global myocardial performance			
LV MPI	0.65 ± 0.10	0.47 ± 0.07	<0.0001
Systolic function			
LV global longitudinal strain, %	-11.0 (4.0)	-11.9 (2.9)	0.264
RV global longitudinal strain, %	-11.5 ± 3.8	-11.4 ± 3.9	0.823
LV ejection time', s*			
Crude	0.16 (0.02)	0.20 (0.02)	<0.0001
Adjusted by cardiac cycle length	0.38 ± 0.05	0.40 ± 0.05	0.017
LV isovolumetric contraction time', s*			
Crude	0.05 ± 0.01	0.05 ± 0.08	0.053
Adjusted by cardiac cycle length	0.12 ± 0.02	0.09 ± 0.02	<0.0001
RV ejection time', s*			
Crude	0.17 ± 0.02	0.22 ± 0.02	<0.0001
Adjusted by cardiac cycle length	0.39 ± 0.05	0.41 ± 0.05	<0.0001
RV isovolumetric contraction time', s*			
Crude	0.05 (0.01)	0.04 (0.05)	<0.0001
Adjusted by cardiac cycle length	0.11 (0.05)	0.08 (0.03)	<0.0001
Diastolic function			
LV E/E' ratio	6.9 (2.5)	7.4 (2.9)	0.144

RV E'/A' ratio	0.7 (0.3)	0.8 (0.4)	0.349
LV relaxation time', s*			
Crude	0.18 ± 0.03	0.22 ± 0.04	<0.0001
Adjusted by cardiac cycle length	0.40 (0.07)	0.41 (0.08)	0.472
LV isovolumetric relaxation time', s*			
Crude	0.05 ± 0.01	0.04 ± 0.01	0.008
Adjusted by cardiac cycle length	0.11 (0.03)	0.09 (0.02)	<0.0001
RV relaxation time', s*			
Crude	0.17 ± 0.03	0.21 ± 0.05	<0.0001
Adjusted by cardiac cycle length	0.40 ± 0.05	0.41 ± 0.08	0.320
RV isovolumetric relaxation time', s*			
Crude	0.05 (0.02)	0.05 (0.01)	0.130
Adjusted by cardiac cycle length	0.11 (0.04)	0.09 (0.02)	<0.0001

Data are mean ± SD, or median (interquartile range). LV, left ventricular; RV, right ventricular; IVS, inter-ventricular septum; MPI, myocardial performance index obtained by PW Doppler technique; E, passive early diastolic peak velocity obtained by PW Doppler; A, atrial contraction diastolic peak velocity obtained by PW Doppler; S', systolic annular peak velocity by PW-TDI; E', early diastolic annular peak velocity by PW-TDI; A', atrial contraction diastolic annular peak velocity by PW-TDI; *, values adjusted by cardiac cycle length.

Table S3. Perinatal changes in regional longitudinal strain and systolic strain rate

Measurements	Fetal	Neonatal	P
LV segmental longitudinal strain, %			
Basal septum	-11.4 ± 5.6	-15.4 ± 5.0	<0.0001
Mid septum	-9.3 (5.8)	-11.2 (5.2)	0.084
Apical septum	-11.4 (8.6)	-11.2 (6.8)	0.646
Apical wall	-11.5 (9.2)	-5.0 (5.5)	<0.0001
Mid wall	-9.8 (12.7)	-9.3 (6.8)	0.060
Basal wall	-6.6 (12.9)	-18.5 (8.1)	<0.0001
Global	-11.0 (4.0)	-11.9 (2.9)	0.264
LV segmental longitudinal systolic strain rate, 1/s			
Basal septum	-1.3 (1.0)	-1.3 (0.5)	0.253
Mid septum	-1.2 (0.9)	-0.9 (0.4)	<0.0001
Apical septum	-1.4 (1.0)	-0.9 (0.5)	0.284
Apical wall	-1.3 (1.3)	-0.5 (0.3)	<0.0001
Mid wall	-1.4 (1.5)	-0.7 (0.5)	<0.0001
Basal wall	-1.5 (1.3)	-1.7 (0.9)	0.213
Global	-1.4 (0.9)	-1.0 (0.4)	<0.0001
RV segmental longitudinal strain, %			
Basal septum	-15.5 (17.1)	-19.7 (15.2)	0.096
Mid septum	-11.8 (14.4)	-11.35 (9.3)	0.446
Apical septum	-7.7 (7.1)	-8.7 (9.6)	0.284
Apical wall	-8.0 (7.1)	-5.0 (4.4)	<0.0001
Mid wall	-8.8 (6.3)	-9.8 (6.2)	0.775
Basal wall	-11.1 ± 5.5	-11.62 ± 5.1	0.535
Global	*-11.5 ± 3.8*	*-11.4 ± 3.9*	*0.823*
RV segmental longitudinal systolic strain rate, 1/s			
Basal septum	-1.9 (1.6)	-2.1 (1.5)	0.301
Mid septum	-1.5 (1.2)	-1.1 (0.6)	<0.0001
Apical septum	-0.9 (0.7)	-0.7 (0.5)	<0.0001
Apical wall	-1.4 (0.8)	-0.6 (0.3)	<0.0001
Mid wall	-1.0 (0.7)	-0.7 (0.3)	<0.0001
Basal wall	-1.2 (0.8)	-1.1 (0.5)	<0.0001
Global	-1.5 (0.7)	-1.0 (0.6)	<0.0001

Data are mean ± SD, or median (interquartile range). LV, left ventricular; RV, right ventricular.

Table S4. Intra- and inter-observer errors of fetal and neonatal cardiac indices

Measurements	Fetal		Neonatal	
	ICC>0.7	LoA, p>0.05	ICC>0.7	LoA, p>0.05
Intra-observer measurement error (same frame), N=50				
All measurements	44/50 (88%)	47/50 (94%)	44/50 (88%)	43/50 (86%)
B-, M-mode, PW Doppler	16/20 (80%)	19/20 (95%)	18/20 (90%)	18/20 (90%)
Tissue Doppler imaging	12/12 (100%)	12/12 (100%)	12/12 (100%)	11/12 (92%)
Speckle tracking imaging	16/18 (89%)	16/18 (89%)	14/18 (78%)	14/18 (78%)
Intra-observer overall error (different frame), N=50				
All measurements	39/50 (78%)	46/50 (92%)	44/50 (88%)	45/50 (90%)
B-, M-mode, PW Doppler	16/20 (80%)	18/20 (90%)	18/20 (90%)	18/20 (90%)
Tissue Doppler imaging	11/12 (92%)	12/12 (100%)	11/12 (92%)	11/12 (92%)
Speckle tracking imaging	12/18 (67%)	16/18 (89%)	14/18 (78%)	16/18 (89%)
Inter-observer measurement error (same frame), N=20				
All measurements	26/30 (87%)	29/30 (97%)	22/30 (73%)	29/30 (97%)
Tissue Doppler imaging	12/12 (100%)	12/12 (100%)	12/12 (100%)	12/12 (100%)
Speckle tracking imaging	14/18 (78%)	17/18 (94%)	10/18 (56%)	17/18 (94%)
Inter-observer overall error (different frame), N=20				
All measurements	20/30 (67%)	26/30 (87%)	23/30 (77%)	28/30 (93%)
Tissue Doppler imaging	10/12 (83%)	11/12 (92%)	12/12 (100%)	12/12 (100%)
Speckle tracking imaging	10/18 (55%)	16/18 (89%)	11/18 (61%)	16/18 (89%)

Data are presented as n/N (%). N, patient number; ICC, intra-class correlation coefficient;

LoA, limits of agreement (Pitman's test)

SUPPLEMENTARY REFERENCES

1. Tutschek B, Schmidt KG. Techniques for assessing cardiac output and fetal cardiac function. *Semin Fetal Neonatal Med*. 2011;16:13-21.

2. Godfrey ME, Messing B, Cohen SM, Valsky DV, Yagel S. Functional assessment of the fetal heart: a review. *Ultrasound Obstet Gynecol*. 2012;39:131-44.

3. Van Mieghem T, DeKoninck P, Steenhaut P, Deprest J. Methods for prenatal assessment of fetal cardiac function. *Prenat Diagn*. 2009;29:1193-203.

4. Cruz-Lemini M, Crispi F, Valenzuela-Alcaraz B, Figueras F, Sitges M, Gomez O, et al. Value of annular M-mode displacement vs tissue Doppler velocities to assess cardiac function in intrauterine growth restriction. *Ultrasound Obstet Gynecol*. 2013;42:175-81.

5. Jain A, Mohamed A, El-Khuffash A, Connelly KA, Dallaire F, Jankov RP, et al. A comprehensive echocardiographic protocol for assessing neonatal right ventricular dimensions and function in the transitional period: normative data and z scores. *J Am Soc Echocardiogr*. 2014;27:1293-304.

6. Brooks PA, Khoo NS, Mackie AS, Hornberger LK. Right ventricular function in fetal hypoplastic left heart syndrome. *J Am Soc Echocardiogr*. 2012;25:1068-74.

7. Hernandez-Andrade E, Benavides-Serralde JA, Cruz-Martinez R, Welsh A, Mancilla-Ramirez J. Evaluation of conventional Doppler fetal cardiac function parameters: E/A ratios, outflow tracts, and myocardial performance index. *Fetal Diagn Ther*. 2012;32:22-9.

8. DeVore GR. Assessing fetal cardiac ventricular function. *Semin Fetal Neonatal Med*. 2005;10:515-41.

9. Hecher K, Campbell S, Snijders R, Nicolaides K. Reference ranges for fetal venous and atrioventricular blood flow parameters. *Ultrasound Obstet Gynecol*. 1994;4:381-90.

10. Cruz-Martinez R, Figueras F, Bennasar M, Garcia-Posadas R, Crispi F, Hernandez-Andrade E, et al. Normal reference ranges from 11 to 41 weeks' gestation of fetal left modified myocardial performance index by conventional Doppler with the use of stringent criteria for delimitation of the time periods. *Fetal Diagn Ther*. 2012;32:79-86.

11. Hernandez-Andrade E, Figueroa-Diesel H, Kottman C, Illanes S, Arraztoa J, Acosta-Rojas R, et al. Gestational-age-adjusted reference values for the modified myocardial performance index for evaluation of fetal left cardiac function. *Ultrasound Obstet Gynecol*. 2007;29:321-5.

12. Lobmaier SM, Cruz-Lemini M, Valenzuela-Alcaraz B, Ortiz JU, Martinez JM, Gratacos E, et al. Influence of equipment and settings on myocardial performance index repeatability and definition of settings to achieve optimal reproducibility. *Ultrasound Obstet Gynecol*. 2014;43:632-9.

13. Hernandez-Andrade E, Lopez-Tenorio J, Figueroa-Diesel H, Sanin-Blair J, Carreras E, Cabero L, et al. A modified myocardial performance (Tei) index based on the use of valve clicks improves reproducibility of fetal left cardiac function assessment. *Ultrasound Obstet Gynecol*. 2005;26:227-32.

14. Comas M, Crispi F, Gomez O, Puerto B, Figueras F, Gratacos E. Gestational age- and estimated fetal weight-adjusted reference ranges for myocardial tissue Doppler indices at 24-41 weeks' gestation. *Ultrasound Obstet Gynecol*. 2011;37:57-64.

15. Acharya G, Pavlovic M, Ewing L, Nollmann D, Leshko J, Huhta JC. Comparison between pulsed-wave Doppler- and tissue Doppler-derived Tei indices in fetuses with and without congenital heart disease. *Ultrasound Obstet Gynecol*. 2008;31:406-11.

HIGHLIGHTS

- Establish feasibility of assessing fetal and neonatal cardiac function.
- Perinatal period is associated with major changes in fetal ventricular geometry and cardiac function in response to significant alterations in loading conditions.
- Improved knowledge of perinatal cardiac changes in normal fetuses could facilitate better understanding of cardiac adaptation in normal and pathological pregnancies.